Fabrication of Ni^{2+} incorporated ZnO photoanode for efficient overall water splitting

Humaira Rashid Khan[a,b,c], Bilal Akram[d], Muhammad Aamir[a], Muhammad Azad Malik[b,*], Asif Ali Tahir[c], Muhammad Aziz Choudhary[a], Javeed Akhtar[a,**]

[a] *Materials Laboratory, Department of Chemistry, Mirpur University of Science and Technology (MUST), -10250 AJK, Pakistan,*
[b] *School of materials, The University of Manchester,, School of Materials, The University of Manchester, Oxford Road, Manchester M13 9PL, UK, Manchester, 10250, Pakistan*
[c] *Environment and Sustainability Institute (ESI), University of Exeter Penryn,, Cornwall,, UK, TR10 9FE, UK*
[d] *Department of Chemistry, Tsinghua University, Beijing 100084, China, 100084, china*

Email: Azad.malik@manchester.ac.uk , javeed.chem@must.edu.pk

Abstract

In this work, we present an effective and facile approach for deposition of zinc oxide, and nickel incorporated zinc oxide thin films to fabricate photoanode of photoelectrochemical cell. Incorporation of Ni^{2+} in the host ZnO matrix results in the dramatic shape evolution of the resulting films from simple bullet like structures to complex punch like microstructures with increased estimated electrochemically active surface area. In addition to the role of Ni^{2+} in structure determination, it significantly enhanced the photoelectrochemical performance by improving the charge transport properties and conductivity of the parent host matrix. This work demonstrates a move towards tailoring functional properties of the films via controlled incorporation of different ionic species. This simple incorporation scheme can further be applied to attain a variety of compositionally tunable unique structures for desired applications by judiciously adjusting precursor choices and manipulating relative concentrations of the incorporated precursors during growth.

Key words: ZnO, Nickel doping, PEC, AACVD, Tofel plot

Introduction

With the growing utilization of fossil fuels and the release of greenhouse gases, the development of novel technologies for green and sustainable energy creation has been considered as one of the top priorities for mankind. Photoelectrochemical (PEC) water splitting, a route to solar energy transformation and storage in chemical bonds, provides an emerging approach for production of renewable hydrogen fuel and environmental remediation.[1, 2] To meet such a challenging target, development of a stable and efficient photocatalyst to carry out overall water splitting without using any sacrificial agents or any external potential is the ultimate goal.[3]

Since the revolutionary founding work of PEC water splitting by TiO_2 as the photoanode in 1972,[4, 5] hydrogen production through PEC technology has engrossed immense attention and a variety of materials has been investigated for their PEC performance such as TiO_2, ZnO, WO_3,α-Fe_2O_3,[6] $BiVO_4$,[7] BiO_X (X=Cl, Br ,I),Cu_2O.[8] Among these different materials ZnO has earned much attention because of Zinc metal is cost effective, copious, and non-toxic and can show excellent electrical properties.[9-13] Zinc oxide (ZnO) is a typical UV-active *n*-type semiconductor material having a hexagonal wurtzite crystal structure with a direct band gap of about 3.33 eV.[14, 15] The distinctive electron mobility in ZnO is 10-100 times superior than that of TiO2 which is favorable for electron transport during PEC water splitting. Moreover, the unique polar surfaces of ZnO make it best among the series. Taking the over potential requirements (0.4-0.6 eV) and energy losses (0.3-0.4 eV) during PEC water splitting into account, a perfect band gap should be 2.0 eV, analogous to a light absorption rim of 620 nm.[16-18]

Therefore attempts were being made to tailor the band gap of a semiconductor by external incorporation of other atomic or ionic species of an element. The incorporation of any specie into the crystal structure leads either to the donor states close to the conduction band in case of n-type conductivity or acceptor states close to the valence band in case of *p*-type character of conductivity.[19]High levels of doping (concentration in order of $1x10^{20}$ cm^3) can give rise to low resistivity which eventually leads to high plasma resonance reflectivity and high free carrier absorption, consequently in poor transmission. This may appear austere but the electrical conduction can be improved via enhancing the carrier mobility whilst retaining the optical transmission. This will be attained by getting better film's microstructure, lowering

"killer" concentrations of defects and reducing the scattering centers of impurity.[20] Insights on the growth of the external species incorporated microstructures is still limited even though attempts aiming to explore the underlying mechanisms which control incorporation have been reported in the literature.[21-23] In spite of these attempts, the interactions between incorporated species and host crystal lattices in the growth of mixed micro and nanocrystals are still unclear. Studies on the influence of so-called dopants in shape de- termination of nanostructures and microstructures are rare.[24] As a result, shape control of mixed nanocrystals is less advanced as compared to plain nanocrystals.[25]

This work explores the employ of Aerosol Assisted Chemical Vapor Deposition (AACVD) of ZnO and Ni:ZnO thin films as a cost effective and facile substitute to conventional deposition techniques such as APCVD, sol gel, DC/RF sputtering, and spray pyrolysis to fabricate photoanode.[26-30]

Herein, we report that in the AACVD growth of ZnO thin films microstructures, incorporation of Ni species results in dramatic shape evolution in addition to the compositional disparity of the resultant films. Depending on the relative concentrations of the Ni precursor, Ni incorporated ZnO thin films microstructures with well-defined shapes, from sheet like structures to complex punch like microstructures, which display adoptable optoelectronic characteristics, were obtained for the first time. Thin film electrodes are further investigated for their photoelectrochemical properties and tunable performance can be achieved via compositional variation and spatial complexity. Moreover, this approach to fabricate photoanode is simple and doesn't need post-deposition treatments like annealing/calcination for improving grain boundaries as in the case of sol-gel and spin coating

Material and methods

All chemicals were used as received without any additional purification. The thin films of pristine and nickel incorporated ZnO were deposited on glass substrate by using home- built aerosol assisted chemical vapor deposition method (AACVD). The experimental setup de- tailed description and of AACVD is reported (earlier) elsewhere.[31],[32] Briefly, the precursor solution was prepared by mixing varying concentrations (2%, 5%, 10% and 15%) of nickel acetate tetrahydrate with zinc acetate dihydrate in 20 mL methanol solution. The resulting solution was transferred to two necked round bottom flask and placed in water bath above an ultrasonic humidifier where the aerosols were generated. The aerosols were transferred to the

reaction chamber by using argon as a carried gas with the reaction temperature set at 400°C for 2 hours. In order to check the photoelectrochemical water splitting performance, same procedure of thin films deposition was repeated using FTO substrate.

Characterizations

The crystallinity and phase of the as-deposited thin films were characterized by D8 ADVANCE XRD (Bruker, Germany) using Cu.Kα radiation (λ = 1.54178 Å′).The chemical composition and surface morphology of the as-deposited thin films were investigated by field emission scanning electron microscope (FESEM) (TESCAN MIRA3XMU, JEOL, USA) attached with an energy dispersive X-ray spectroscopy (EDX) instrument. SHIMADZU UV 1800 Spectrophotometer was applied for the diffused reflectance of as de- posited thin films of pristine and $Zn_{1-x}Ni_xO$ (x= 0.02, 0.05, 0.10 and 0.15) thin films.

Photoelectrochemical Study

In a typical photoelectrochemical water splitting experiment, three-electrode system was used for the measurement in which 1 M $Na_2SO_4$was used as an electrolyte with Ni-ZnO/FTO as working electrode, a Pt wire as a counter electrode and Ag/AgCl reference electrode in a 5 mL quartz cell thus making a three electrode system. Ni-ZnO/FTO photoelectrode was dipped in electrolyte solution while the bare area of the photoelectrode was kept above the level of electrolyte and was used to develop the electrical contact with a gold-plated clip. During measurements, light was allowed to pass through a quartz window and subsequently it travelled to the electrolyte before falling on the surface of Ni-ZnO photoelectrode. The illuminated surface area of photoelectrode was estimated ~ 1.6 cm^2. The AM 1.5 class A solar simulator (Solar Light 16S - 300 solar simulator) was used as standard light source. The voltage scan speed was kept at 0.05 V/s during measurements for consistent results .Further , the light was manually chopped using a card board of thickness ~ 2cm at regular intervals of 3 seconds/cycle to monitored photocatalytic efficiency of as-prepared photoelectrodes.[33]

The cyclic voltammetry (CV) curves were measured at a scan rate of 0.05 V/s with a voltage range of about 0.1 to 0.5 V. The chronoamperometric measurements were used for the evaluation of the photo stability and durability of the as-deposited photoanodes under chopped light illumination condition for 900 seconds. Electrochemical measurements were carried out using an Auto lab PGSTAT12 potentiostat and the electrode potential is changed to the reversible hydrogen electrode (RHE) by using the following relation.[34]

$E°_{AgCl} = +0.197$ V at 25°C

Results

The structural features of as deposited films were investigated through SEM. Fig. 1 a-j reveals the morphology of plain ZnO and Ni doped ZnO. Specifically, a very uniform bullets like structures were obtained in case of plain ZnO, Fig. 1(a -b) which changes largely upon doping. As the concentration of Nickel ion increases the morphological evolution occurs from sheet like structures in case of 2 % Fig.1 (c-d) to complex punch like microstructures in case of maximum that is 15 % Fig.1 (i-j) through intermediate hierarchical flowers like structures in case of 5% and 10 % as shown in Fig.1 (e-f) and (g-h) respectively. It is worth mentioning that all the deposited films have very uniform and homogeneous microstructures that are arranged regularly on the substrates. The elemental composition of a representative films containing 15 % Ni as a dopant is shown in Fig. 1(k). It can be seen that all the elements are uniformly distributed in the whole film microstructures.

Sets of reactions with different molar ratios of nickel acetate in the reagents were conducted to systematically study the doping effects on the resulting microstructures of the films. As shown in Fig. 2, the shape evolution of the doped ZnO films is evident. By incorporating nickel in the ZnO matrix, the morphology of as-deposited thin films varied largely and it can be inferred that it is the Ni which effect the morphology rather than the acetate ligand. As in case of plain ZnO there is 100% acetate from ZnOAc source and in case of doped ZnO we have used the same acetate source precursor of the nickel and obtained different morphology. On the basis of this observation it can be assumed that it is the Ni ion which determine the geometry of the resulting films microstructures. Moreover, the morphology of the films is more sensitive to Ni^{+2} content as it gets changed with change in the precursor concentration. The change in morphology is reliable with the fact that incorporation of nickel ion into the host lattice alters the growth pathway through initial seedling however the exact mechanism is not clear at the moment.

Fig. 3 shows the X-ray diffraction (XRD) patterns of as- deposited plain ZnO and nickel incorporated ZnO thin films fabricated by AACVD method. The diffraction peaks at 2θ values

of 31.82, 34.33, 36.49 and 47.56, which correspond to (100), (002), (101) and (102) planes of hexagonal wurtzite structure (ICPDS No. 086254). It was observed that with increase in nickel concentration the intensity of peaks decreases gradually from as-deposited $Zn_{0.98}Ni_{0.02}O$ to $Zn_{0.85}Ni_{0.15}O$ thin films. Similarly, there is slight shift in peak positions on incorporation of nickel in the ZnO matrix which may be attributed due to slight difference between ionic radii of Ni^{+2}(0.069 Å) and Zn+2(0.72 Å). A shift towards lower values indicate the formation of defects in the lattices of resulting films.[35]

The optical properties of as deposited thin films vary greatly upon Ni incorporation that can be evident through their physical appearance. Ni incorporated ZnO is brown in color which gets even more darker upon increase in Ni concentration in reagents as compared to plain ZnO which is white in color (Fig. 4a). Diffuse reflectance spectroscopy (DRS) was used to estimate the optical band gap of plain ZnO and nickel incorporated ZnO thin films with different concentrations (2%, 5%, 10% and 15%) shown in fig. 4(b). It was observed that as-deposited pristine ZnO shows the absorption at 391 nm. With incorporation of varying concentrations of nickel, a shift towards longer wavelength was observed in the absorption spectra from 395 nm for $Zn_{0.98}Ni_{0.02}O$ to 413 nm for $Zn_{0.85}Ni_{0.15}O$ thin films. This shift may be because of good interaction between the oxides of Ni^{+2} and Zn^{+2} i.e. due to the interaction of d-electrons of Ni ions with the s and p electrons of ZnO.[36]

Kubelka-Munk method was applied to determine the band gap of as-deposited thin films and were shown in fig. 4(c). The band gap of pristine ZnO was found to be 3.2 eV and was reduced to 2.18 eV for $Zn_{0.85}Ni_{0.15}O$ thin films. This reduction of bandgap may be due to the difference of ionic radii between Ni^{+2}(0.69 Å) and Zn^{+2}(0.74Å).[37]Similarly, as Ni^{+2}occupies the interstitial sites of ZnO matrix, the formation of intrinsic band results in the reduction of band gap due to the interaction between 4d orbital of nickel with 2p orbital of oxygen, which rearranged fermi level to valence band.[38]

The PEC water splitting performances of the photoanodes was examined by using three electrode system in 0.1 M Na_2SO_4solution with as grown plain and Ni incorporated ZnO@FTO as working electrode. Pt wire as a counter electrode and Ag/AgCl reference electrode in a 5 mL quartz cell.

Fig. 5(a) shows the current density- voltage (J-V) plots of the as deposited plain ZnO and

$Zn_{1-x}Ni_xO$ (x=2%, 5%, 10%and15%) photo anodes under light and dark conditions. All the thin films show very low current densities under dark. Upon irradiation, plain ZnO shows limited photoelectrochemical activity with a current density of about 3.46 x10^{-4} A/cm^2 at 0.2V. On nickel incorporation with varying concentrations (2%, 5%, 10% and15%), the photo current density is enhanced which shows that all nickel incorporated ZnO photoanodes showed photocurrent density higher than the plain ZnO. The increase in current density was from 5.1 x 10^{-4}A/cm^2 for $Zn_{0.98}Ni_{0.02}O$ to 1.7 x 10^{-3}A/cm^2at 0.2 V for $Zn_{0.85}Ni_{0.15}O$ photoanodes. This increase in current density for the nickel incorporated ZnO thin films confirms the function of nickel as an efficient electrocatalysts for PEC activity.

The kinetics of photoelectrochemical performance[39, 40] for pristine ZnO and nickel incorporated ZnO thin films in terms of Tafel plot were calculated and shown in fig.5c.The values of Tafel slope for plain ZnO photoelectrode was found to be 1220 mV/dec. (Upon incorporation of different concentrations of nickel into the ZnO matrix, the slop vales decrease gradually from 1074, 1034, 824,813mV/dec respectively for $Zn_{1-x}Ni_xO$ (x=0.02, 0.05, 0.10 and 0.15). In order to know the factors responsible for superior performance of a catalyst their specific active surface area was estimated. The double layer capacitance (cdl)in cyclic voltammetry curves (CV) was used to determine the effective active surface areas of nickel incorporated ZnO photoelectrodes at different nickel concentrations.[41]Fig. 5d shows the CV curves of $Zn_{1-x}Ni_xO$ (x =0.02, 0.05, 0.10 and 0.15) at different scan rates (0.1, 0.15, 0.2, 0.25, 0.3, 0.35, 0.4, 0.45 and 0.5). The Cdl values of all the as-deposited photoelectrodes can be estimated by plotting Δj (j_a-j_c) versus the scan rate from the CV curve. The calculated values of Cdl for $Zn_{0.98}Ni_{0.02}O$, $Zn_{0.95}Ni_{0.05}O$, $Zn_{0.90}Ni_{0.10}O$, and $Zn_{0.85}Ni_{0.15}O$ were 91.07 mF/cm^2, 100.99 mF/cm^2, 137.34 mF/cm^2 and 187.37 mF/cm^2respectively. Apparently, $Zn_{0.85}Ni_{0.15}O$ showed increased Cdl value than all other photoelectrodes, representing great exposure of effective active sites. This increasing trend in surface area can be attributed to their special geometry.[40]

Amperometric studies were carried out for as-deposited plain ZnO and $Zn_{1-x}Ni_xO$ (x= 2%, 5%, 10% and 15%) thin films, in 0.1 M Na_2SO_4electrolyte at an applied potential of 0.5 V vs RHE under light on-off cycles for 900 sec. Fig. 6 reveals that there is no apparent decrease in the photocurrent density for all the photoanodes, which proves the stability of as fabricated photoanodes. It is important to note that on sudden illumination, all the photoanodes show

photocurrent spike which may be because of the bulk separation of excited electron-hole pairs stored at the interface of electrolyte and semiconductor. Hence, the formation of spikes can be applied for the measurement of the lifetime of the charge carrier of the photoanodes which in turn is related to the overall rate of charge recombination of the as fabricated thin films. Among all the photoanodes used in the amperometric measurements, $Zn_{0.85}Ni_{0.15}O$ thin films shows maximum vales of photocurrent which is in good agreement of the stability of as deposited photoanode and showed better PEC activity.

In short, Ni ions plays a significant role in determining the geometry of as deposited films microstructures and thus enhancing the photoelectric response in the films. Ni acts as an ionized donor due to the substitution into host lattice. Firstly, the improved donor concentration would result in the enhancement of the conductivity, the improvement of charge transfer, and the decline of carrier recombination. Secondly, the increased donor concentration would increase the electric field across the space charge layer, resulting in higher charge separation efficiency.

Conclusions

AACVD has been shown to be an effective and simple method for the deposition of highly transparent and conductive zinc oxide, and nickel doped zinc oxide films. Control over the carrier mobility, charge-carrier density, reflectance, crystallinity, and the surface morphology of the films have shown to be highly dependent upon the incorporated concentration of Ni using this technique. Incorporation of Ni^{+2} is a critical for the dramatic shape evolution of the Ni-incorporated ZnO films microstructures. High quality Ni: ZnO films with well-defined shapes, from simple bullets like structures to complex punch like microstructures, which exhibit tunable photoelectrochemical properties, have been deposited for the first time by this method. In addition to the role of nickel in structure determination it also plays an important role in photoelectrochemical performance by improving the conductivity and the charge transport properties of the parent host matrix in ZnO. This work demonstrates a move towards tailoring functional properties of the films via controlled incorporation of nickel. This simple scheme can further be applied to obtain a variety of compositionally tuneable unique structures for desired applications by judiciously adjusting precursor choices and manipulating relative concentrations of the incorporated precursors during growth.

Acknowledgements

Hk thanks HEC for IRSIP fellowship. JA thanks HEC Pakistan for funding (Grant#8227, NRUP/R&D/HEC-2018/19). MAZ acknowledges Higher education commission (HEC) grant# 7181/AJK/NRUP/R&D/HEC-2017

References

[1] T. Faunce, S. Styring, M.R. Wasielewski, G.W. Brudvig, A.W. Rutherford, J. Messinger, A.F. Lee, C.L. Hill, M. Fontecave, D.R. MacFarlane, Artificial photosynthesis as a frontier technology for energy sustainability, Energy & Environmental Science, 6 (2013) 1074-1076.

[2] R. Kant, S. Pathak, V. Dutta, Design and fabrication of sandwich-structured α-Fe2O3/Au/ZnO photoanode for photoelectrochemical water splitting, Solar Energy Materials and Solar Cells, 178 (2018) 38-45.

[3] M. Zhu, Z. Sun, M. Fujitsuka, T. Majima, Z-Scheme Photocatalytic Water Splitting on a 2D Heterostructure of Black Phosphorus/Bismuth Vanadate Using Visible Light, Angewandte Chemie International Edition, 57 (2018) 2160-2164.

[4] A. Fujishima, K. Honda, Electrochemical photolysis of water at a semiconductor electrode, nature, 238 (1972) 37.

[5] R.-B. Wei, P.-Y. Kuang, H. Cheng, Y.-B. Chen, J.-Y. Long, M.-Y. Zhang, Z.-Q. Liu, Plasmon-enhanced photoelectrochemical water splitting on gold nanoparticle decorated ZnO/CdS nanotube arrays, Acs Sustainable Chemistry & Engineering, 5 (2017) 4249-4257.

[6] B.-F. Zheng, T. Ouyang, Z. Wang, J. Long, Y. Chen, Z.-Q. Liu, Enhanced plasmon-driven photoelectrocatalytic methanol oxidation on Au decorated α-Fe 2 O 3 nanotube arrays, Chemical Communications, 54 (2018) 9583-9586.

[7] J.W. Park, M.A. Mahadik, G.W. An, S.Y. Lee, G. Piao, S.H. Choi, W.-S. Chae, H.-S. Chung, H. Park, J.S. Jang, Activation of a highly oriented columnar structure of ZnFe2O4 for photoelectrochemical water splitting: Orchestrated effects of two-step quenching and Sn4+ diffusion, Solar Energy Materials and Solar Cells, 187 (2018) 207-218.

[8] B. Akram, K. Ahmad, J. Khan, B.A. Khan, J. Akhtar, Low-temperature solution-phase route to sub-10 nm titanium oxide nanocrystals having super-enhanced photoreactivity, New Journal of Chemistry, 42 (2018) 10947-10952.

[9] S. Chen, T. Takata, K. Domen, Particulate photocatalysts for overall water splitting, Nature Reviews Materials, 2 (2017) 17050.
[10] Y. Tachibana, L. Vayssieres, J.R. Durrant, Artificial photosynthesis for solar water-splitting, Nature Photonics, 6 (2012) 511.
[11] G. Liu, H.G. Yang, J. Pan, Y.Q. Yang, G.Q. Lu, H.-M. Cheng, Titanium dioxide crystals with tailored facets, Chemical reviews, 114 (2014) 9559-9612.
[12] G. Liu, C.Y. Jimmy, G.Q.M. Lu, H.-M. Cheng, Crystal facet engineering of semiconductor photocatalysts: motivations, advances and unique properties, Chemical Communications, 47 (2011) 6763-6783.
[13] Z. Zhang, J.T. Yates Jr, Band bending in semiconductors: chemical and physical consequences at surfaces and interfaces, Chemical reviews, 112 (2012) 5520-5551.
[14] X. Yang, A. Wolcott, G. Wang, A. Sobo, R.C. Fitzmorris, F. Qian, J.Z. Zhang, Y. Li, Nitrogen-doped ZnO nanowire arrays for photoelectrochemical water splitting, Nano letters, 9 (2009) 2331-2336.
[15] A. Murphy, P. Barnes, L. Randeniya, I. Plumb, I. Grey, M. Horne, J. Glasscock, Efficiency of solar water splitting using semiconductor electrodes, International journal of hydrogen energy, 31 (2006) 1999-2017.
[16] M. Xiao, S. Wang, S. Thaweesak, B. Luo, L. Wang, Tantalum (oxy) nitride: narrow bandgap photocatalysts for solar hydrogen generation, Engineering, 3 (2017) 365-378.
[17] M. Xiao, B. Luo, M. Lyu, S. Wang, L. Wang, Single-Crystalline Nanomesh Tantalum Nitride Photocatalyst with Improved Hydrogen-Evolving Performance, Advanced Energy Materials, 8 (2018) 1701605.
[18] C. Zhen, R. Chen, L. Wang, G. Liu, H.-M. Cheng, Tantalum (oxy) nitride based photoanodes for solar-driven water oxidation, Journal of Materials Chemistry A, 4 (2016) 2783-2800.
[19] H. Hartnagel, A. Dawar, A. Jain, C. Jagadish, Semiconducting transparent thin films, Institute of Physics Bristol, 1995.
[20] D.S. Bhachu, G. Sankar, I.P. Parkin, Aerosol assisted chemical vapor deposition of transparent conductive zinc oxide films, Chemistry of Materials, 24 (2012) 4704-4710.
[21] G.M. Dalpian, J.R. Chelikowsky, Self-purification in semiconductor nanocrystals, Physical review letters, 96 (2006) 226802.
[22] S.C. Erwin, L. Zu, M.I. Haftel, A.L. Efros, T.A. Kennedy, D.J. Norris, Doping semiconductor nanocrystals, Nature, 436 (2005) 91.

[23] D. Chen, R. Viswanatha, G.L. Ong, R. Xie, M. Balasubramaninan, X. Peng, Temperature dependence of “elementary processes” in doping semiconductor nanocrystals, Journal of the American Chemical Society, 131 (2009) 9333-9339.
[24] L. Zu, D.J. Norris, T.A. Kennedy, S.C. Erwin, A.L. Efros, Impact of ripening on manganese-doped ZnSe nanocrystals, Nano letters, 6 (2006) 334-340.
[25] R. Viswanatha, D.M. Battaglia, M.E. Curtis, T.D. Mishima, M.B. Johnson, X. Peng, Shape control of doped semiconductor nanocrystals (d-dots), Nano Research, 1 (2008) 138-144.
[26] P. Gerhardinger, D. Strickler, Fluorine doped tin oxide coatings-over 50 years and going strong, in: Key engineering materials, Trans Tech Publ, 2008, pp. 169-178.
[27] R.G. Palgrave, I.P. Parkin, Aerosol assisted chemical vapor deposition using nanoparticle precursors: a route to nanocomposite thin films, Journal of the American Chemical Society, 128 (2006) 1587-1597.
[28] K. Choy, Chemical vapour deposition of coatings, Progress in materials science, 48 (2003) 57-170.
[29] S. O'Brien, M.G. Nolan, M. Çopuroglu, J.A. Hamilton, I. Povey, L. Pereira, R. Martins, E. Fortunato, M. Pemble, Zinc oxide thin films: Characterization and potential applications, Thin Solid Films, 518 (2010) 4515-4519.
[30] S. Oda, H. Tokunaga, N. Kitajima, J.-i. Hanna, I. Shimizu, H. Kokado, Highly oriented ZnO films prepared by MOCVD from diethylzinc and alcohols, Japanese journal of applied physics, 24 (1985) 1607.
[31] M.D. Khan, M. Aamir, M. Sohail, M. Sher, J. Akhtar, M.A. Malik, N. Revaprasadu, Novel single source precursor for synthesis of Sb 2 Se 3 nanorods and deposition of thin films by AACVD: Photo-electrochemical study for water reduction catalysis, Solar Energy, 169 (2018) 526-534.
[32] A.F. Butt, M.H. Bhatti, M. Aamir, M.N. Tahir, M. Sher, M.J. Ahmed, J. Akhtar, A Facile Synthesis of Organotin (IV) Carboxylates: Application as Single Source Precursor for Deposition of Tin Oxide Thin Films and Evaluation of Biological Activities, ChemistrySelect, 3 (2018) 10325-10332.
[33] Z. Chen, H.N. Dinh, E. Miller, Photoelectrochemical water splitting, Springer, 2013.
[34] A.A. Tahir, K.U. Wijayantha, S. Saremi-Yarahmadi, M. Mazhar, V. McKee, Nanostructured α-Fe2O3 thin films for photoelectrochemical hydrogen generation, Chemistry of Materials, 21 (2009) 3763-3772.
[35] I.N. Reddy, C.V. Reddy, A. Sreedhar, J. Shim, M. Cho, K. Yoo, D. Kim, Structural, optical,

and bifunctional applications: Supercapacitor and photoelectrochemical water splitting of Ni-doped ZnO nanostructures, Journal of Electroanalytical Chemistry, 828 (2018) 124-136.
[36] I. Ahmad, M. Mazhar, M. Usmani, K. Khan, S. Ahmad, J. Ahmad, Synthesis, characterization and photocatalytic performance investigation of nickel doped ZnO nanoparticles, Digest Journal of Nanomaterials and Biostructures, 13 (2018) 1149-1157.
[37] I. Kang, M.J. Schulz, J.H. Kim, V. Shanov, D. Shi, A carbon nanotube strain sensor for structural health monitoring, Smart materials and structures, 15 (2006) 737.
[38] F. Xu, Y. Yuan, D. Wu, M. Zhao, Z. Gao, K. Jiang, Synthesis of ZnO/Ag/graphene composite and its enhanced photocatalytic efficiency, Materials Research Bulletin, 48 (2013) 2066-2070.
[39] X. Tong, P. Yang, Y. Wang, Y. Qin, X. Guo, Enhanced photoelectrochemical water splitting performance of TiO_2 nanotube arrays coated with an ultrathin nitrogen-doped carbon film by molecular layer deposition, Nanoscale, 6 (2014) 6692-6700.
[40] R.A. Mir, O.P. Pandey, Influence of graphitic/amorphous coated carbon on HER activity of low temperature synthesized β-Mo_2C@ C nanocomposites, Chemical Engineering Journal, 348 (2018) 1037-1048.
[41] M.A. Lukowski, A.S. Daniel, F. Meng, A. Forticaux, L. Li, S. Jin, Enhanced hydrogen evolution catalysis from chemically exfoliated metallic MoS_2 nanosheets, Journal of the American Chemical Society, 135 (2013) 10274-10277.

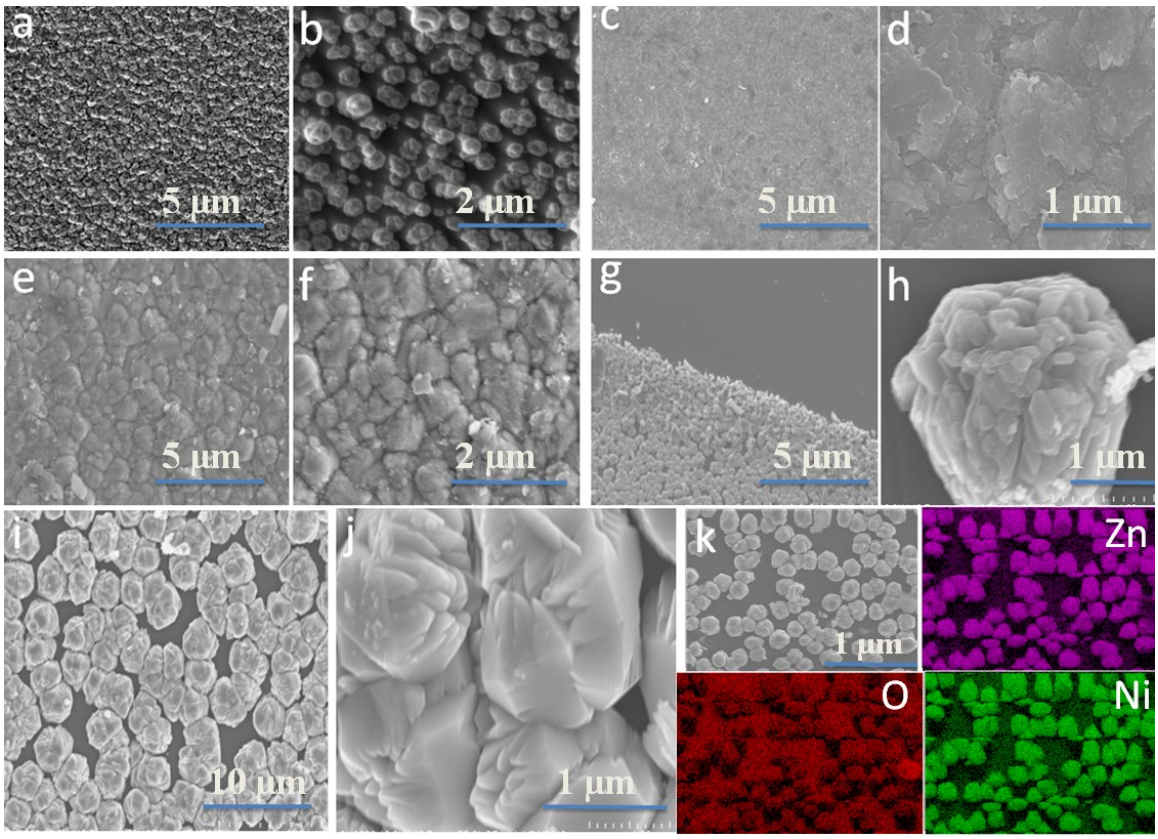

Fig. 1 SEM images of as-deposited (a,b) plain ZnO, (c,d)2% Ni doped ZnO,(e,f) 5% Ni doped ZnO, (g, h) 10% Ni doped ZnO, and (i, j) 15% Ni doped ZnO thin films grown by AACVD method. Fig 1k reveals the elemental distribution through EDX of a representative sample obtained through addition of 15 % Ni precursor in the reagent

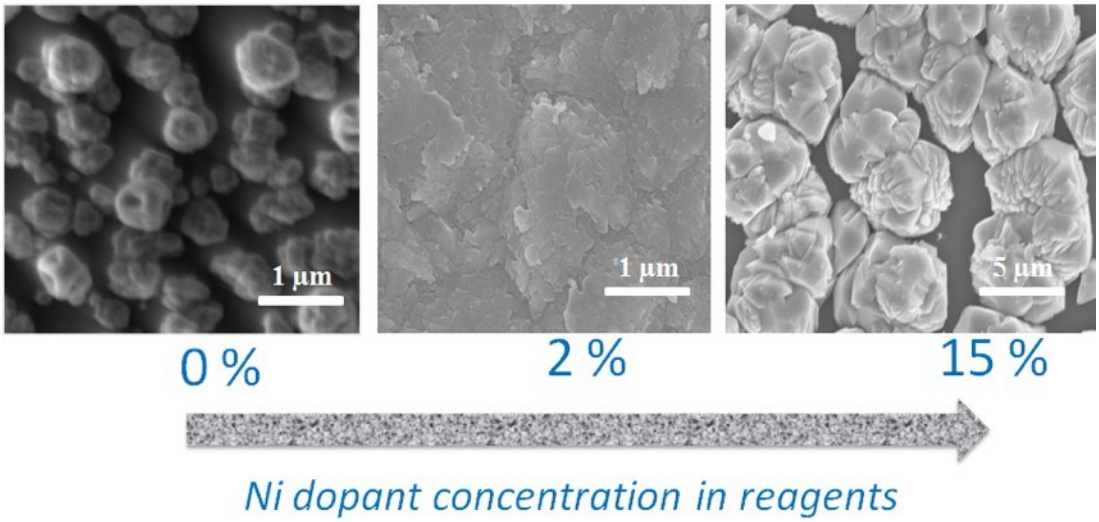

Fig. 2 Representative SEM images of the nanocrystals from the 0%,2% and 15% Ni acetate reactions, emphasizing the shape evolution of films microstructures due to the increasing Ni dopant concentrations in the reagents(highlighted by the arrow).

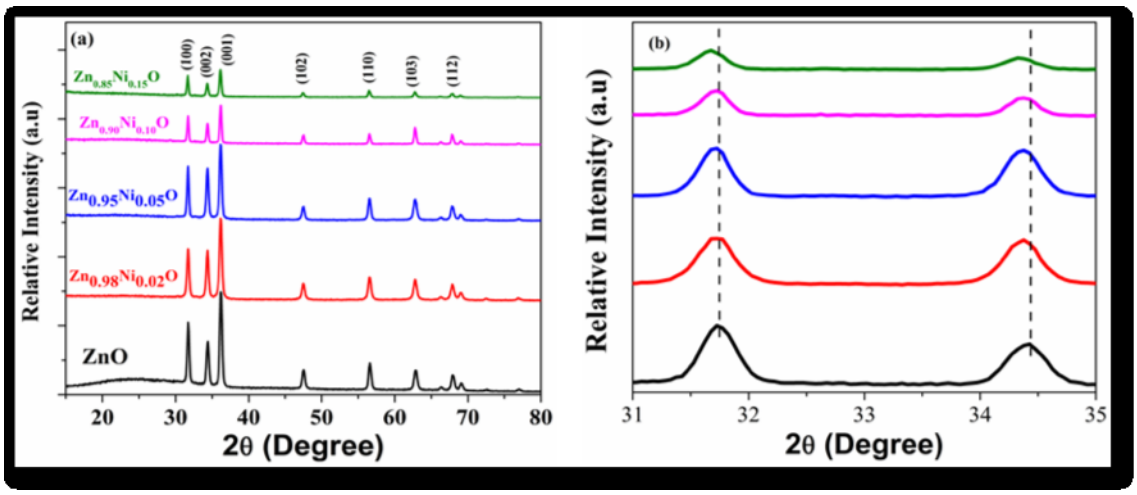

Fig. 3 (a) Comparative pXRD patterns of plain ZnO and Zn1−xNixO (x= 0.02, 0.05, 0.10 and 0.15) thin films, (b) Zoom-in pXRD spectra of as-deposited films showing diffraction peaks shifting.

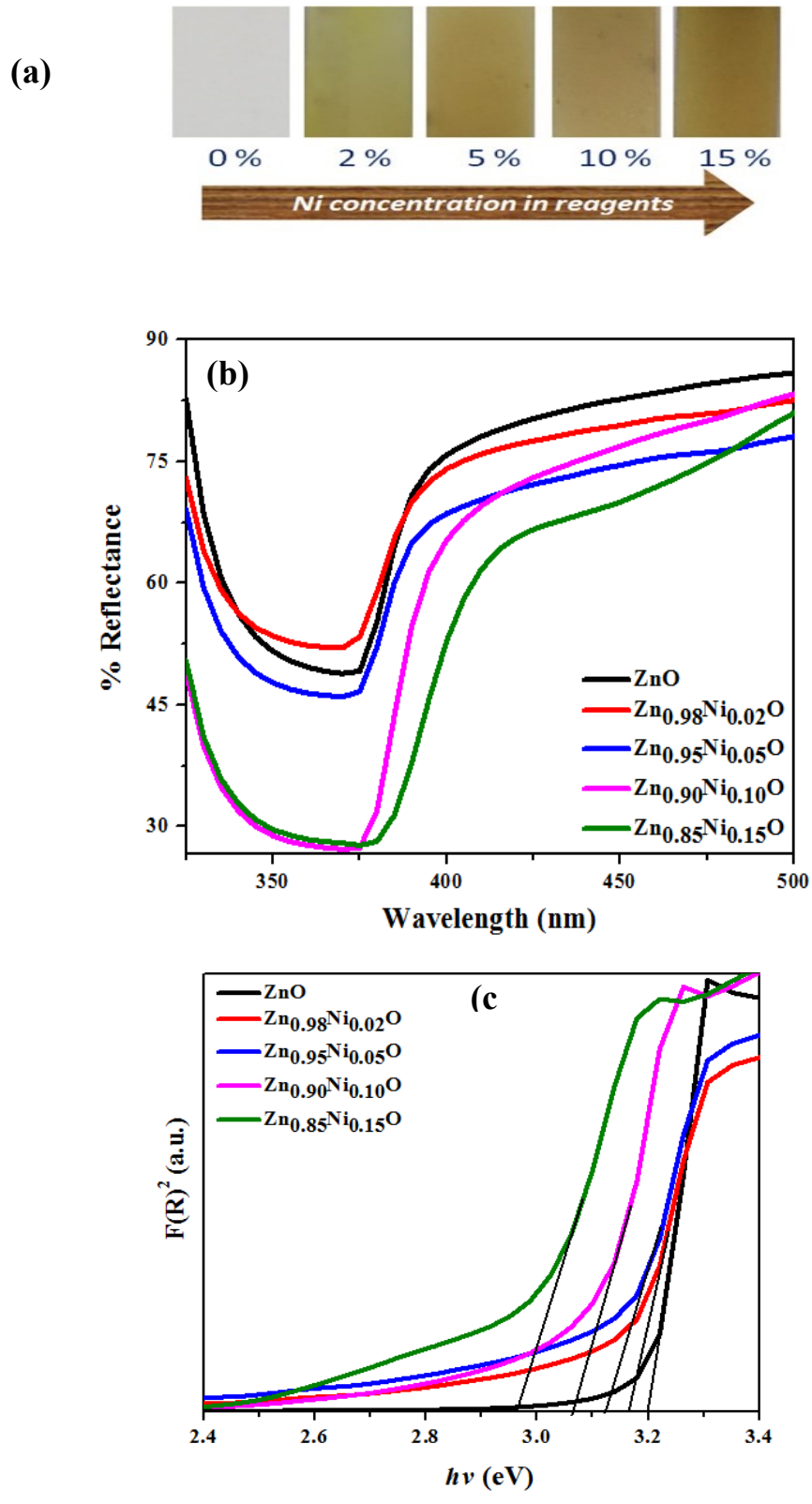

Fig. 4 (a) Digital photograph of as-deposited thin films by AACVD on FTO substrates (b) Diffused Reflectance spectra (c) Band gap calculated from Kubelka-Munk method for Plain ZnO and Ni incorporated ZnO thin films.

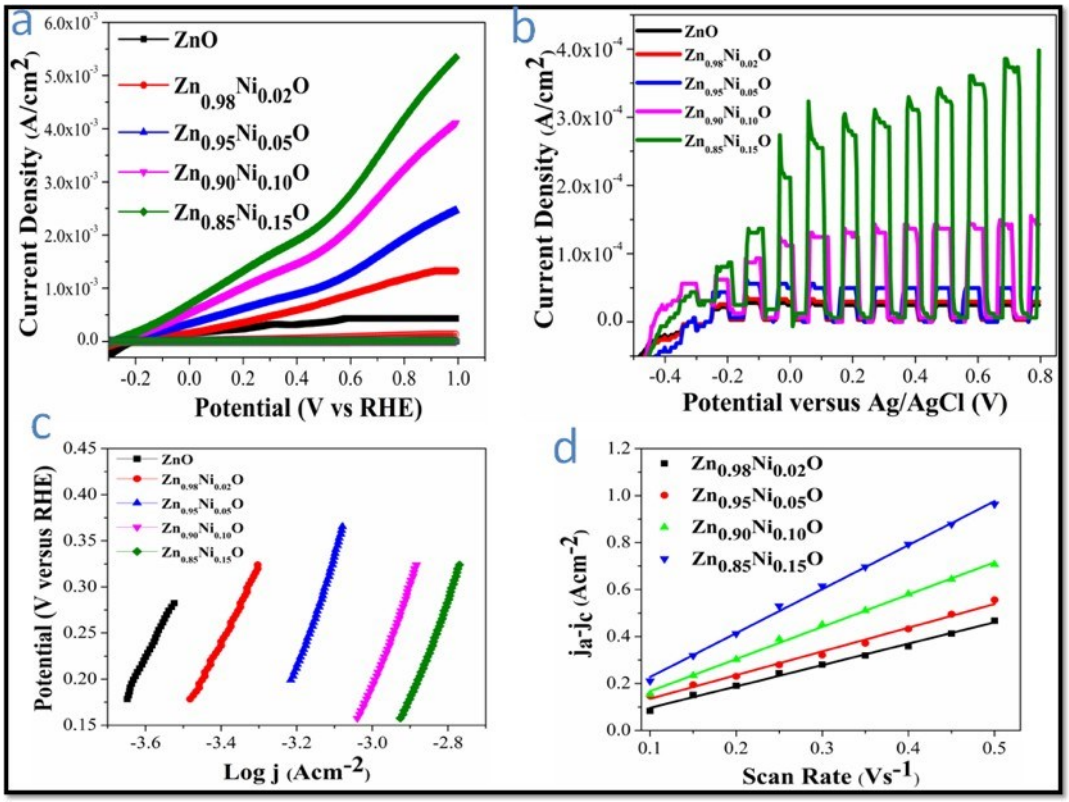

Fig. 5 (a) Photocurrent potential curves in light and dark (The solid symbols reveals performance in light whereas corresponding hollows symbols shows photoelectrochemical behavior in dark) (b) Chopped in light and dark conditions for plain ZnO and Nickel incorporated ZnO.(c)Tafel plots of different catalyst and (d) Difference between cathodic and anodic current versus various scan rates for as-deposited $Zn1-xNixO$ photoelectrodes.

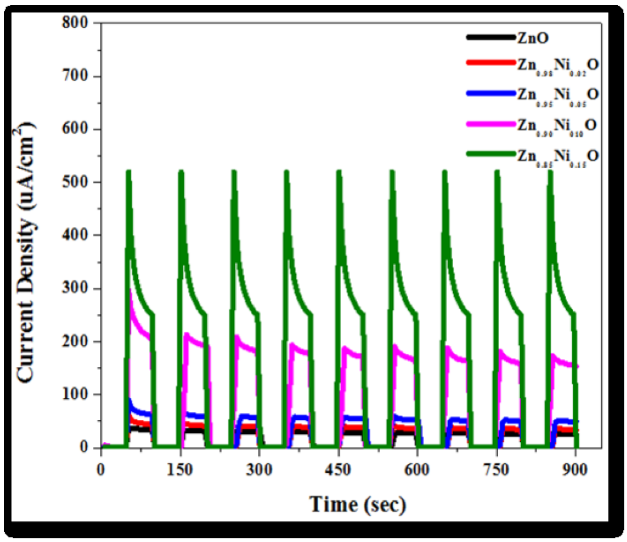

Fig. 6 Amperometric I-t curves for as deposited ZnO and Nickel incorporated ZnO thin films in 0.1 M Na_2SO_4 electrolyte at an applied potential under light on-off cycles for 900 sec.